The gravitational influence of satellite Pan on the radial distribution of ring–particles in the region of the Encke–division in Saturn's A ring

F. Spahn
Working group "Nonlinear Dynamics" (MPG)
University Potsdam; D-O-1571 Potsdam; Germany

J.-M. Petit
C.N.R.S.
Observatoire de Nice, B.P. 229, 06304, Nice cedex 04, France

Ph. Bendjoya
Observatoire de Nice, B.P. 229, 06304, Nice cedex 04, France

Abstract

Here we summarize the models and their similarities with respect to the gravitational influence of small satellites (moonlets) embedded in planetary rings, which have been developed by Petit and Hénon (1987a,b; 1988) and by Spahn (1987; Spahn et al. 1989; 1992). The results and their applicabilities are shown in the case of the Encke–gap Moon Pan located in the outer A–ring of Saturn's rings. To compare the model–profiles with the experimental ones (optical depth profile measured by Voyager–photopolarimeter), the structures embedded in the latter have been confirmed statistically using the "wavelet" analysis method. This analysis points to a size of Pan of about 13 km and an eccentricity of 10^{-4} of its orbit.

1 Motivation

Much work has been done with respect to the gravitational action of satellites - embedded and outer ones - on planetary rings, which have culminated in the prediction and detection of the satellite Pan in the Encke division of Saturn's rings (Showalter et al. 1986; Showalter 1991).

In this paper we will give a brief summary of the work done concerning the question: " What is the gravitational influence of a small satellite (moonlet) on the radial density distribution of ring–material in the close radial surrounding of its orbit ?"

In Section 2 we summarize the models developed by Petit and Hénon (1987a; b; 1988; hereafter PH 1; 2; 3), and by Spahn (1987; Spahn and Wiebicke 1989; Spahn et al. 1992; hereafter S 1; 2; 3). We enlighten the similarities of the models and the good agreement of a few of their results, which then will be taken together to look for moonlet-like structures in the Voyager occultation data. This is especially done in Section 3 where we compare the results of the models with the radial density- profiles of Saturn's rings measured by the Photopolarimeter (PPS) of Voyager 2 at the Encke division of Saturn's ring where satellite Pan has been discovered recently. This gives a possibility to prove directly the value of the results of the models. Therefore the information about the real structure in the rings has to be separated from the large noise of the PPS-data. This has been realized with the wavelet analysis method which yields a noise-reduced optical depth profile.

In Section 4 the results of the comparison between model and experiment will be discussed and also a small overview of still remaining work can be found there.

2 The models

The main common assumptions of either approaches (PH 1; 2; 3; S 1; 2; 3) are:

1. plane motion of all bodies (planet, moonlet, ring-particles);
2. a narrow radial region is considered (compared to the whole radial extension of the rings);
3. the standard-model of spherical, undestructible ring-particles has been applied.

With these assumptions, both models has been applied in order to solve the problem of the gravitational influence of the embedded moonlet on the time-evolution of the radial distribution of ring-particles in the close vicinity (region of overlapping resonances) of the orbit of the perturbing moon. That distribution is given by the function $f(m,r,t)$, $f.dm.dr$ being the number of particles in the radial interval $[r, r+dr]$ and in the mass-range $[m, m+dm]$ at a given time t. Then the evolution of $f(m,r,t)$ can be written by mean of a continuity equation

$$\partial_t f(m,r,t) = \hat{\mathbf{A}}(f,r,t) \cdot f \tag{1}$$

in a very general form.

For more details concerning the meaning of Eq. (1) we refer to the derivation of equation (44) in PH2 and of equation (3) in S2.

The operator $\hat{\mathbf{A}}$ governs the radial transport of the ring–matter and is generally dependent on the gravity of the perturbing moonlet, as well as the interactions between the ring–particles - gravity and direct physical collisions - represented by the dependency of $\hat{\mathbf{A}}$ on f itself (PH2; 3). The integro-differential equation (1) is of a fairly complicated form which makes it impossible to get a general analytical solution. Therefore numerical approaches have been used (PH; S) in order to solve this equation for special cases, e.g. single and bimodal size distributions.

The advantage of the model developed by Petit and Hénon (1987a; b; 1988) is the wide physical generality taken into account in equation (1), which is presented by including:

a) arbitrary size distribution of the ring-particles;

b) particle interactions $\Rightarrow$ gravity and direct inelastic collisions (fixed coefficient of restitution $\epsilon = constant < 1$; see PH1).

The price for this wide generality is a relatively low number of particles - $N = 500 \cdots 1000$ - taken for the numerical treatment of Eq. (1), which gives a fairly rough resolution of the final radial density profiles.

Such resulting profiles are shown in the fig. 1 for the special case of a bimodal size (mass) distribution for the ring- particles (one moonlet and many much smaller particles). The time evolution of the radial particle distribution is given for a comparatively massive moonlet. In this case the moonlet is able to create an empty gap which is divided by a faint ringlet, covering the orbit of the moonlet (fig. 1f). The ringlet consists of particles in "tadpole" and "horseshoe" orbits (Dermott and Murray 1981). Of high importance is the fact that Petit and Hénon (1988) have been able to obtain an equilibrium width of the gap created by the moonlet, that is a result of the balance between the torque exerted from the moonlet to the ring–material and the torque caused by the particle interactions itself (viscous torque; see also Lissauer et al. 1981). They obtained for that width W:

$$W \approx \begin{cases} M_m^{1/3}, & \text{for} \quad M_m < M_0, \\ M_m^{2/3}, & \text{for} \quad M_m \geq M_0, \end{cases} \tag{2}$$

where M_0 is the mass threshold depending on the different model parameter (PH3). The order of magnitude is $M_0 \approx 10^{13} kg$ which corresponds to a size of an icy moonlet of a diameter $D \approx 2.7 km$.

In the model of Spahn (1987; S2; S3) particle interactions have been neglected and only the gravitational influence of the moonlet on the ring–material near its orbit has been taken into account. This simplification has enabled to consider (S3):

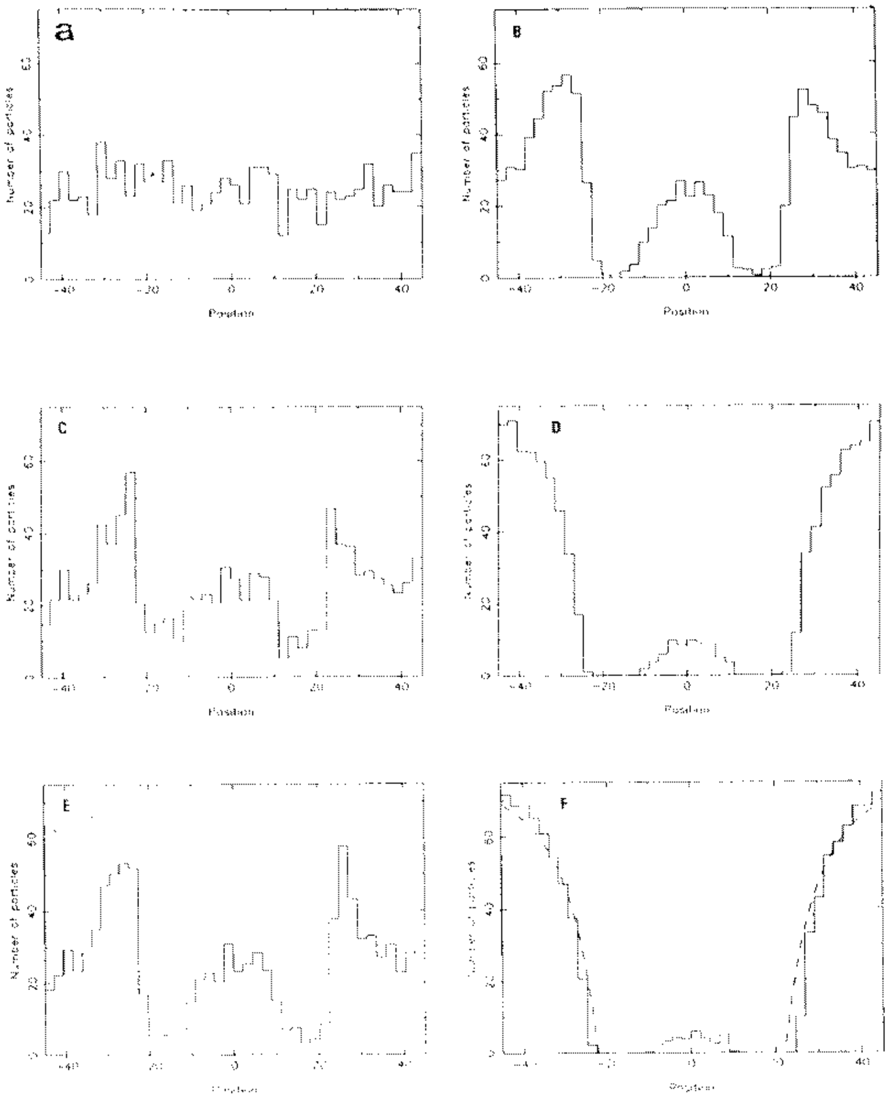

Fig. 1: Time evolution of the radial distribution of very small particles ($m \ll M_m$) around the orbit of a moonlet at the "position"$= 0.0$. The different parts belong to snapshots at different elapsed time of the computer-experiment. Clearly visible is the formation of a gap which is separated by a faint ringlet around the "position"$= 0.0$ (Figure taken from PH3).

1. $N = 5000 \cdots 50,000$ particles, giving a high radial resolution of the density profiles;

2. n (up to three) co-orbital moonlets of different masses;

3. eccentric orbits of the moonlets.

However in that model no equilibrium width of the created gap can be expected because of the neglect of the particle interactions - no viscous torque is counteracting the torque exerted by the moon. Here the advantage is to study in detail the dependency of the shape (radial profile) and the width of the inner ringlet on the orbital motion of a massive moonlet ($M_m > M_0$). Concerning the mass-dependence of the radial density profile Spahn and Wiebicke (1989) have obtained results comparable to Petit and Hénon (1988). Assuming a given random motion of the ring–particles (expressed by a mean orbital eccentricity $\overline{e}$; S2), caused by particle interactions and additional outer perturbations (Goldreich and Tremaine 1978; PH1), the inner ringlet is vanishing with decreasing mass of the moonlet M_m, while the gap-width scales as "$W \propto M_m^{1/3}$". For very massive moonlets ($h \approx [M_m/3M_p]^{1/3} \approx R_m/[km] \cdot 10^{-4} \gg \overline{e}, \quad \overline{e} \leq 10^{-6}$, M_p, R_m and h are the mass of the planet, the radius and the Hill-scale of the moonlet, respectively), the inner ringlet is surprisingly stable and exhibits a detailed structure.

Furthermore, because of the comparable large number of particles $N = 5000 \cdots 50,000$ it has been found (S3), that the density–profile of the inner ringlet shows a detailed structure which contains information about orbital parameters of the moonlet. This is shown in fig. 2, where the different radial density–profiles - taken after a few synodic periods when the structure changes only slightly in time - correspond to different eccentricities e_m of the orbit of the moonlet. Obviously, the larger e_m the narrower the width of the ringlet becomes, which is quite easily seen in fig. 2d where the ringlets caused by moonlet in a circular orbit (solid line), and originated by a moonlet in an eccentric orbit ($e_m = 1.5h$; dashed line), are compared directly. The width W_r of the ringlet can be written

$$W_r \approx C(e_m) \cdot a_m \cdot h(M_m), \tag{3}$$

where a_m is the semi–major axis of the orbit of the moonlet. The factor $C(e_m)$ is a nearly linearly decreasing function of e_m and takes values $C(e_m = 0) \approx 3.0 \cdots C(e_m = 1.5h) \approx 1.2$. At the same time the double-peaked shape of the ringlet-profile turns to a triple peaked one with increasing eccentricity e_m .

Summarizing, the results for

1. the gap-formation and its equilibrium–width (Eq. (2)) of Petit and Hénon (1988);

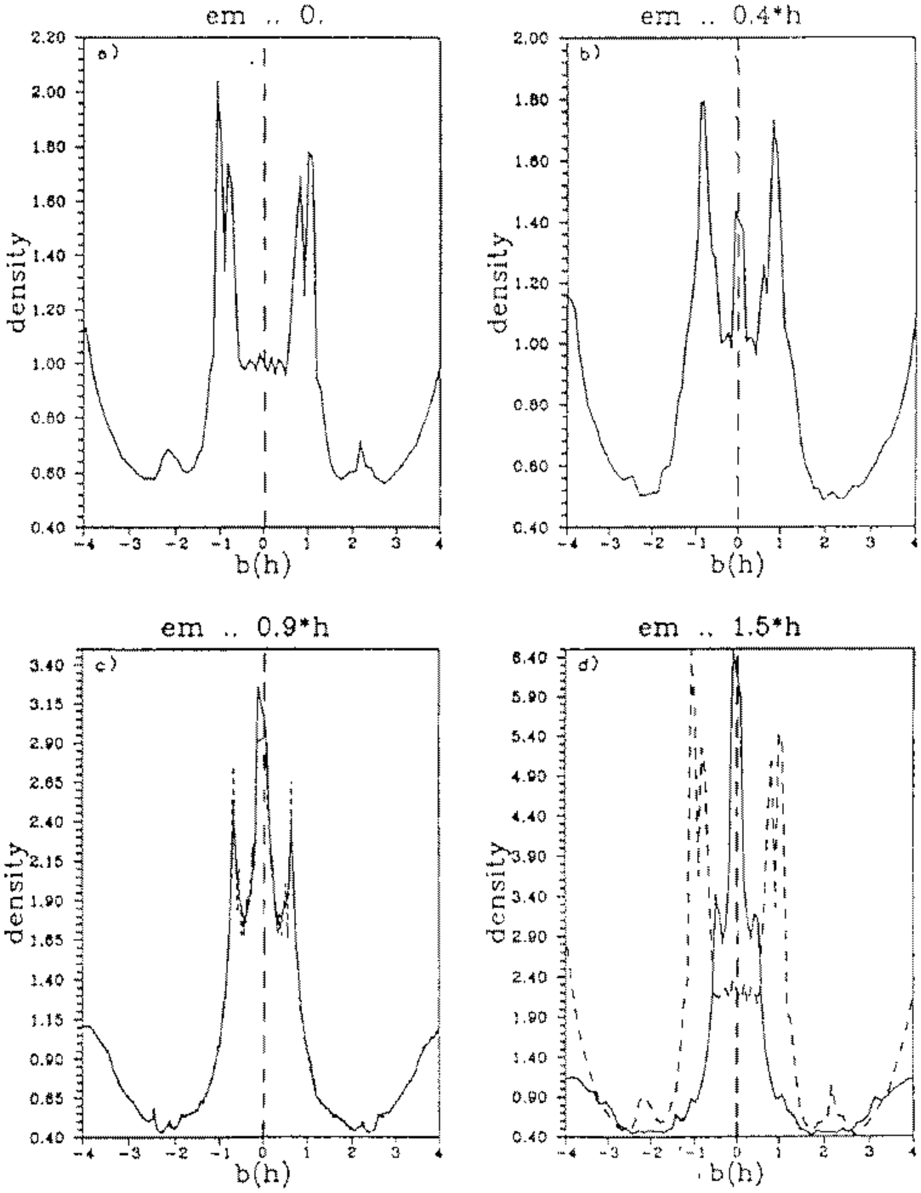

Fig. 2: Radial profiles of $\sigma(b, t = constant)$ (b - impact parameter) for different eccentricities e_m of the orbit of the moonlet (case of a "cold" ring $\Rightarrow$ mean-eccentricity of the ring-particles $\overline{e} \rightarrow 0$). A narrowing of the ringlet-width is really obvious, and furthermore the shape of the density-profile is turning from a double peaked to a triple peaked one with increasing e_m. All profiles show a quasi-symmetry $\sigma(b) \approx \sigma(-b)$ with respect to the orbit of the moonlet at $b = 0.0$.

2. the information about the ringlet found by Spahn et al. (1992) (the ringlet-width and the shape of its density-profile);

3. as well as the fact that all profiles obtained (PH 3; S2; 3) are quite symmetric with respect to the mean radial location of the moonlet-orbit, according to $\sigma(b) \approx \sigma(-b)$;

could now be used to search for small embedded satellites. Before doing this in a future work, the value of the above findings will be tested in the case of satellite Pan, embedded in the Encke–gap of Saturn's rings. This is presented in the next section.

3 The action of satellite Pan in the Encke-gap

If the results of our models are of any value for the reality, they should be visible also in the optical depth-profile of such a ring-region where a satellite is moving. This is the case for the Encke-division in the A-ring of Saturn, where Showalter (1991) has discovered recently a new satellite - named Pan. Fig. 3 shows the optical depth profile $\tau(r)$ of the Encke–division, which has been obtained with the Photopolarimeter (PPS–data) of Voyager 2. At first one recognizes a wide gap - of 315km width - around the orbit of Pan, which is one of the predictions mentioned above (Section 2). Using this value for the width and applying the relation (2) of PH3 we find that one needs a moonlet of mass $M_m \approx 1.2\ 10^{15} kg$ to create such a gap. For an icy moon the corresponding size would be about $D_m \approx 13km$. This satellite would be able to confine a ringlet of a width of $W_r \approx 25km$, if the moon is assumed to move in a circular orbit. The narrowing of the ringlet–width (we see only a 15 km wide ringlet) can be explained by an eccentric orbit of Pan, with an eccentricity of $e_{Pan} \approx h_{Pan} \approx 10^{-4}$ (according to relation (3)). Then the radial profile of the ringlet should be triple–peaked (see fig. 2).

The bottom parts of fig. 3 show enlargements of that ringlet region which correspond to the resolutions of $450m$ and $900m$ (processed by binning the PPS-data), respectively. They seem to have the required symmetry, $\tau(b) \approx \tau(-b)$ and furthermore, the τ-profile of the ringlet seems to have at all resolutions the expected triple–peaked shape. However, the shape of the profile of the ringlet is in fact not sure because of the large fluctuations of the PPS–data in the Encke–division.

To weight the structure seen in the ringlet-profile we carried out a modified t-test, which seemed to favour the significance of the triple-peaked structure. However, this was not absolutely convincing.

Consequently, to be more sure about the nature of the structure, we have carried out an independent test by applying the wavelet-analysis method.

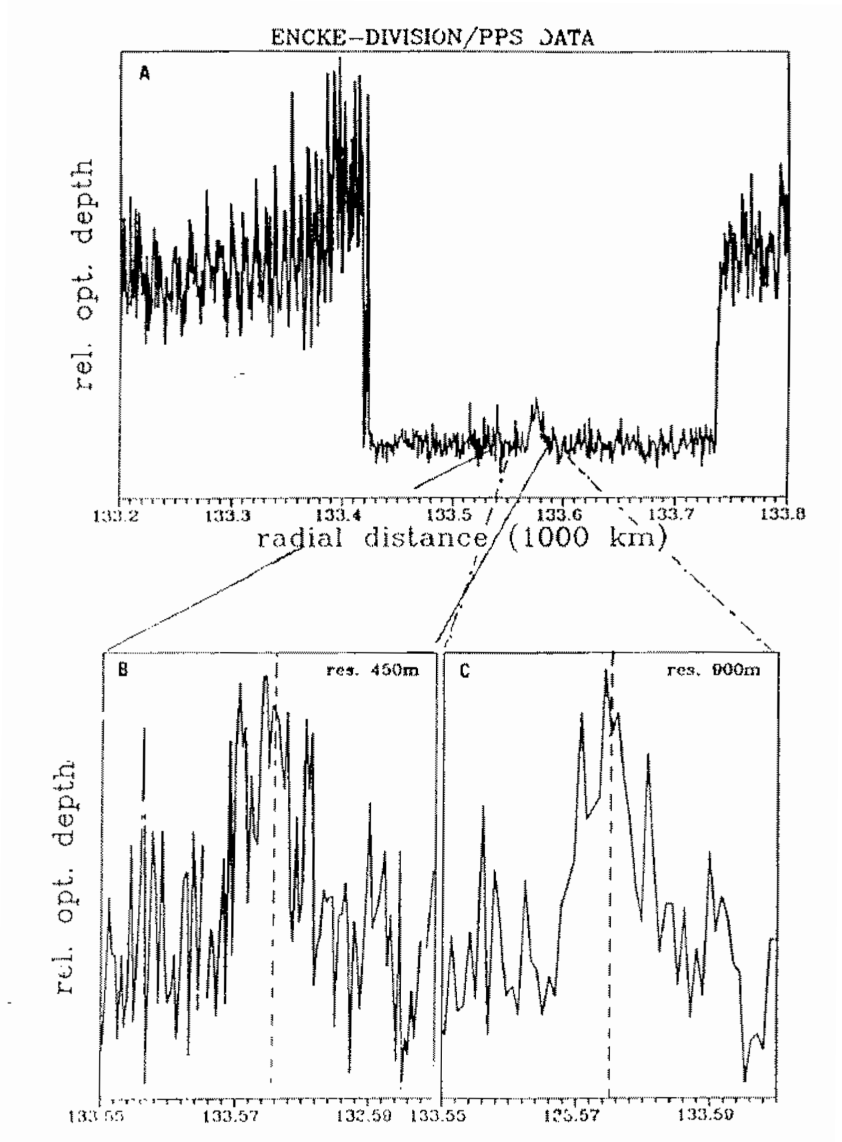

Fig. 3: a) Optical depth profile $\tau(r)$ near the Encke-division in Saturn's A-ring, measured by the Photopolarimeter (PPS) of Voyager 2. Clearly visible: a gap with a faint ringlet at its center, where the orbit of Pan is located. Both features - the gap and the ringlet - have been predicted by the models (see Section 2; PH3, and S1). b-c) Enlargements of the region around the faint ringlet at $450m$ and $900m$ resolution, respectively. Both examples of the ringlet data seem to have the symmetry with respect to the orbit of Pan (vertical dashed lines), and appear to be triple peaked.

The wavelet transform of a signal is the decomposition of this signal onto a basis of functions obtained by dilatations and translations of a unique function called the mother wavelet. It allows to analyse a signal with respect of both a scale parameter and a location parameter, so that it is possible to focus the analysis of the signal at a given location and for a given scale.

Let $s(x)$ be a signal depending only on a space-variable, $\Psi(x)$ the mother wavelet. The wavelet transform of $s(x)$ is then a two variable function $C(a,b)$ depending on a scale variable a and on a location variable b:

$$C(a,b) = \langle s(x), \psi_{a,b}(x) \rangle \qquad \text{with} \qquad \psi_{a,b} = \frac{1}{a}\Psi(\frac{x-b}{a}) \tag{4}$$

where $\langle h(x), g(x) \rangle = \int_{-\infty}^{+\infty} h(x) g^*(x) dx$ and where $g^*(x)$ denotes the complex conjugate of $g(x)$. $C(a_0, b_0)$ can be seen as the details present in $s(x)$ at the scale a_0 in the vicinity of b_0. A wavelet is a zero mean function and rapidly vanishing, which insures from a practical point of view a good localization both in space and scale. From the wavelet transform it is then possible to reconstruct the signal through a reconstruction formula (see Grossmann and Morlet 1985). Our aim has been to use the wavelet transform as a signal processing tool to extract the behavior of the signal in the vicinity of the ringlet, the noise having been removed. The range of considered scales has been chosen in a geometrical progression:

$$a_{i+1} = a_i * 2^{1/12}$$

which insures a practically continuous analysis in scale (see Grossmann et al. 1987), a_0 and a_{max} being defined in order to consider the signal from its step of sampling to its mean. In order to make cross comparisons, two analysing wavelets have been chosen: the mexican hat and the french hat (see Bendjoya and Slezak 1992) which are well suited for hole or structure detections. As preliminary encouraging results we will only present here the reconstruction obtained with the mexican hat wavelet. It is to be noticed that the french hat wavelet analysis gives quite comparable results and will be published later (see Bendjoya et al. 1992).

For each scale a_i, a wavelet coefficient is computed at each point of the sampled signal and to reach our goal we have to eliminate the non significant coefficients and also the scales corresponding to the statistically estimated noise. One disposes then of a set of coefficients on a range of scale which allows to reconstruct without noise the behavior of the signal on this range of scales.

Therefore, we determine the scales corresponding to the noise then we define a threshold for the coefficients scale by scale. Then we have a set of wavelet coefficients on a range of scales not taking into account the noise, and moreover only the statistically significant coefficients are

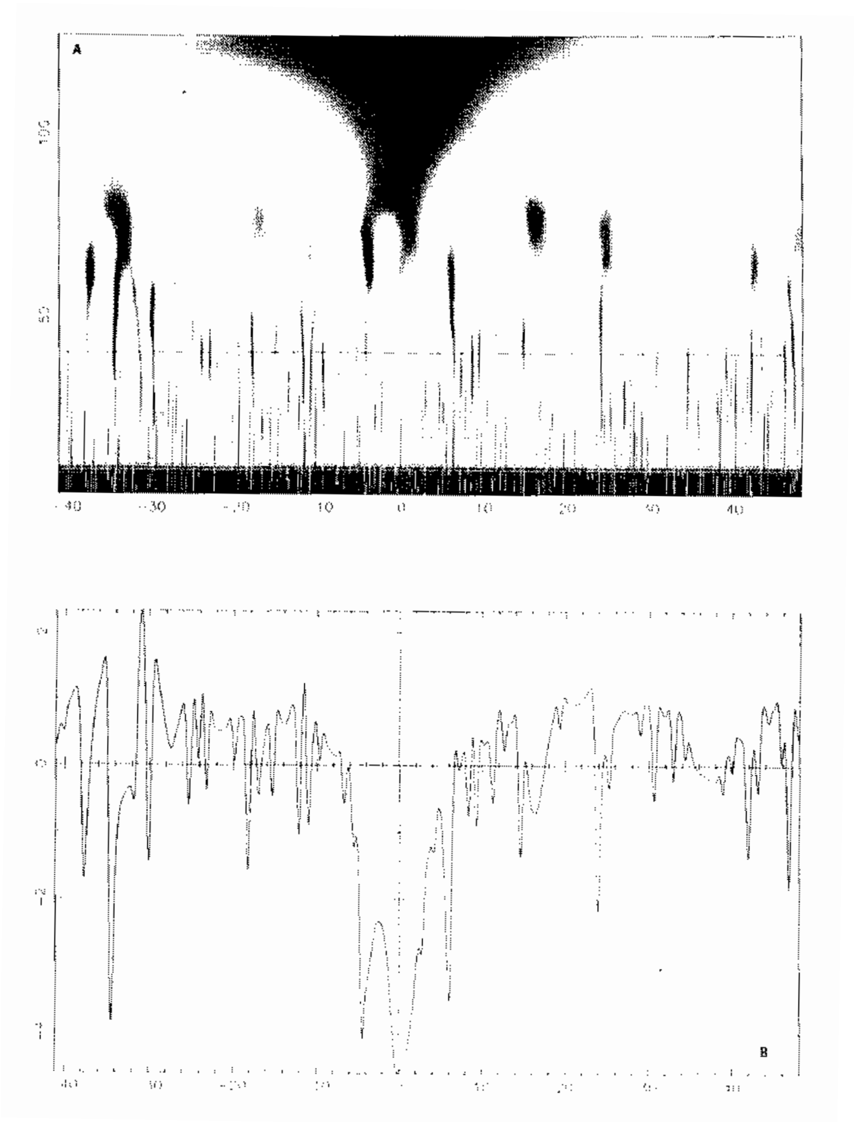

Fig. 4: a) A gray level representation of the wavelet transform of the signal. The x-axis gives the radial distance from the center of the Encke–ringlet (orbital radius of 133 576 km), and the y-axis the scale axis. The coefficient less than the threshold are in gray (black for the smallest ones). The gray levels are renormalized for each scale. The black stripe at the very small scale is due to the sampling effect. The dashed line indicates the limiting scale from which the reconstruction is done. b) The reconstructed photon–count signal. The x-axis is the same as above. The y-axis gives the deviation from the mean photon–count in the Encke–division (no extinction of the star signal). Negative value means extinction, that is presence of ring–material.

considered for each scale. The scale below which everything is considered as noise, and also the thresholds of the wavelet coefficients, are derived from the wavelet analysis of a random signal generated with the constraint to fit the distributions of the values of the PPS signal. For each scale of the wavelet transform of the generated signal we compute the distribution of the coefficients. This strategy allows to decrease significantly and quantify the statistical fluctuations in the wavelet coefficients. The minimum scale to consider for the reconstruction without noise has been evaluated to be a_{40} which corresponds to 250 m. Fig. 4a shows the wavelet transform of this signal displayed in a space-scale plane by a gray level representation. This figure is derived from the PPS–photon–count profile I, which is related to the optical depth by $\tau \propto \ln (I_0/I)$ (I_0 is the photon flux of the occulted star). Since we wanted to detect holes, for each scales the coefficients lower than the threshold are in gray (black for the smallest ones) and the higher ones in white. The dashed line visualizes the scale from which the reconstruction is made. Fig. 4b shows the reconstructed signal from the set of retained coefficients. This reconstruction is made with a threshold at 1- σ. The structure in three peaks of the ringlet appears obviously. It is to be noticed that this peculiar structure persists for more restrictive thresholds. The existence and the symmetry of the ringlet–peaks around the moonlet position as well as the width of the ringlet are in fairly good accordance with the expected results from the model recalled in the second section of this paper. Another ringlet seems also be pointed out by this analysis around the location 133 542 km from the center of Saturn.

4 Discussion

In this paper we have been able to confirm results of theoretical work concerning the gravitational influence of a small satellite, embedded in the rings, on the ring material around its orbit, by analysing the PPS–data of Saturn's rings in the vicinity of the orbit of the satellite Pan. We have been able to estimate the size of Pan to be about $13km$ deduced from the width of the Encke–division, by assuming that the division is swept free by the satellite Pan itself (PH3).

Furthermore, we have compared the shape of PPS–photon–count profile of the Encke–gap–ringlet, as well as its width with theoretical predictions (S3). To do this it has been necessary to remove the noise from the PPS–data in the Encke division, which has been carried out using the wavelet–analysis method. The noise-reduced photon count profile shows three significant depletions inside the ringlet region, pointing to a triple–peaked density profile of the ringlet. This is in accordance with the results of the model and points to an eccentric orbit of Pan - eccentricity $e_m \approx 10^{-4}$. The width of the ringlet confirms the size estimation of Petit and Hénon (1988).

However, the data analysis presented here is only a first step in analysing the radial density profiles of planetary rings. Future work should address the following points:

1. application of different wavelet-functions to the same ring region;

2. refinement of the estimate of the wavelet-coefficient threshold which separates the noise from "real" structures;

3. applying the wavelet-analysis to other rings (or ring regions), where also small satellites are expected to exist.

With respect to the theoretical modelling the following outstanding questions concerning moonlets in planetary rings are of interest:

1. What about the stability of the inner ringlet, if viscous transport processes, sources (the surface of the moonlets) and sinks (meteorite bombardement) of ring matter is taken into consideration?

2. How does the azimuthal distribution of the matter in the ringlet looks like (2D - simulations)?

Both sets of problems will be investigated in subsequent papers.

Acknowledgements

We would like to thank Prof. Larry Esposito, Dr. Karen Simmons, and Dr. Joshua Colwell for providing us with the Voyager-2 PPS-data of planetary rings.

References

[1] Bendjoya, Ph., Petit, J.-M., & Spahn, F., 1993. *Wavelets analysis of the Voyager data on planetary rings. I. Description of the method.* in preparation

[2] Bendjoya, Ph., & Slezak, E., 1992. *Wavelet analysis and applications to some dynamical system.* Celestial Mechanics , in press,

[3] Dermott, S.F., & Murray, C.D., 1981. *The Dynamics of Tadpole and Horseshoe Orbits I. Theory.* Icarus **48**, pp. 1–11.

[4] Goldreich, P., & Tremaine, S., 1978. *The velocity-dispersion in Saturn's rings.* Icarus **34**, pp. 227–239.

[5] Grossmann, A., & Morlet, J., 1985. in *Mathematics+Physics, Lectures on recent results,* ed. L.Streit, World Scientific Publishing,

[6] Grossmann, A., Kronland-Martinet, R., & Morlet, J., 1987. *Reading and understanding continuous wavelet transform.* in *Wavelets, Time-Frequency Methods in Phase Space,* eds. . Combes J.M., Grossmann A. and Tchamitchian Ph., Springer-Verlag, pp. 2–20.

[7] Lissauer, J.J., Shu, F.H., & Cuzzi, J.N., 1981. *Moonlets in planetary rings ?.* Nature **292**, pp. 707–711.

[8] Petit, J.M., & Hénon, M., 1987*a*. *A numerical simulation of planetary rings I. Binary encounters.* Astron. Astrophys. **173**, pp. 389–404.

[9] Petit, J.M., & Hénon, M., 1987*b*. *A numerical simulation of planetary rings II. Monte Carlo model.* Astron. Astrophys. **188**, pp. 198–205.

[10] Petit, J.M., & Hénon, M., 1988. *A numerical simulation of planetary rings III. Mass segregation, ring confinement, and gap formation.* Astron. Astrophys. **199**, pp. 343–356.

[11] Showalter, M., Cuzzi, J.N., Marouf, E.A., & Esposito, L.W., 1986. *Satellite 'wakes' and the orbit of the Encke gap moonlet.* Icarus **66**, pp. 297–323.

[12] Showalter, M., 1991. *Visual detection of 1981 S13, Saturn's eighteenth satellite, and its role in the Encke gap.* Nature **351**, pp. 709–713.

[13] Spahn, F., 1987. *Scattering Properties of a Moonlet (Satellite) Embedded in a Particle Ring: Application to the Rings of Saturn.* Icarus **71**, pp. 69–77.

[14] Spahn, F., & Wiebicke, H.-J., 1989. *Long-Term Gravitational Influence of Moonlets in Planetary Rings.* Icarus **77**, pp. 124–134.

[15] Spahn, F., Saar, A., Schmidt, S. & Schwarz, U., 1992. *The influence of various moonlets on the optical depth profile in planetary rings.* Icarus **100**, pp. 143–153.